COMPRESSIBILITY EFFECTS ON FLOWFIELD STRUCTURE OF TRUNCATED WEDGES IN LOW-DENSITY HYPERSONIC FLOW

Wilson F. N. Santos
National Institute for Space Research
Combustion and Propulsion Laboratory
12630-000, Cachoeira Paulista, SP, Brazil
wilson@lcp.inpe.br

Abstract. Hypersonic flow past truncated wedges at zero incidence in thermal nonequilibrium is investigated for a range of Mach number from 5 to 12. The simulations were performed by using a Direct Simulation Monte Carlo Method. The study focuses the attention of designers of hypersonic configurations on the fundamental parameter of bluntness which can have an impact on even initial design. Some significant differences between sharp and blunt leading edges were noted on the heat transfer coefficient, total drag and on the shock standoff distance. Interesting features observed in the surface fluxes showed that small leading edge thickness compared to the freestream mean free path still has important effects on high Mach number leading edge flows.

Keywords. *DSMC, hypersonic flow, rarefied flow, blunt leading edge, truncated wedge.*

1. Introduction

Hypersonic configurations are generally characterized by slender bodies and sharp leading edges in order to achieve good aerodynamic properties like high lift and low drag. Certain configurations, such as waveriders, are designed analytically with infinitely sharp leading edges for shock wave attachment. Because the shock wave is attached to the leading edge of the vehicle, the upper and lower surfaces of the vehicle can be designed separately. Moreover, the shock wave acts as a valve in order to prevent spillage of higher-pressure airflow from the lower side of the vehicle to the upper side, resulting in a high-pressure differential and enhanced lift.

In addition, for practical hypersonic configurations, leading edges must be blunted for heat transfer, manufacturing, and handling concerns. Because blunt leading edge promotes shock standoff, practical leading edges will have shock detachment, making leading edge blunting a major concern in the design and prediction of flowfields over hypersonic configurations, such as waveriders.

In practice it is extremely difficult to fabricate a perfect sharp tip. Any manufacturing error results in a significant deviation from the design contour and, therefore, sharp edges are difficult to maintain because they are easily damaged. At a more fundamental level, no shape can be made that is perfectly sharp on a molecular scale. There is always some bluntness.

The flowfield properties upstream of the leading edge of a body are affected by molecules reflected from the edge region. The degree of the effect is in part conditioned by the edge geometry. In this context, Santos (2002) investigated the effect of the leading edge thickness on the flowfield structure and on the aerodynamic surface quantities over truncated leading edges. The thickness effect was examined for a range of Knudsen number, based on the thickness of the leading edge, covering from the transitional flow regime to the free molecular flow regime. The emphasis of the work was to provide a critical analysis on maximum allowable geometric bluntness, dictated by either handling or manufacturing requirements, resulting on reduced departures from ideal aerodynamic performance of the vehicle. Thus allowing the blunted leading edge to more closely represent the original sharp leading edge flowfield. Such analysis is also important when a comparison is to be made between experimental results in the immediate vicinity of the leading edge and the theoretical results, which generally assume a zero-thickness leading edge.

Based on recent interest in hypersonic waveriders for high-altitude/low-density applications (Anderson, 1990, Potter and Rockaway, 1994, Rault, 1994 and Graves and Argrow, 2001), this paper extends the analysis presented by Santos (2002). In an effort to obtain further insight into the nature of the flowfield structure of truncated leading edges under hypersonic transitional flow conditions, a parametric study is performed on these shapes with a great deal of emphasis placed on the compressibility effects. In this scenario, the primary goal is to assess the sensitivity of the shock standoff distance, stagnation point heating and the total drag to variations in the freestream Mach number.

For the transitional hypersonic flow, at high Mach number and high altitude, the flow departs from thermal equilibrium and the energy exchange into the various modes due to the vibrational excitation and relaxation becomes important. For the high altitude/high Knudsen number of interest ($Kn > 0.1$), the flowfield is sufficiently rarefied that continuum method is inappropriate. Alternatively, a Direct Simulation Monte Carlo (DSMC) method is used in the current study to calculate the rarefied hypersonic two-dimensional flow on truncated leading edge shapes.

2. Leading Edge Geometry Definition

The truncated wedges to be analyzed in this work are modeled by assuming a sharp leading edge of half angle θ with a circular cylinder of radius R inscribed tangent to this sharp leading edge. The truncated wedges are also tangents to the sharp leading edge and the cylinder at the same common point. The circular cylinder diameter provides a reference for the amount of blunting desired on the leading edges. It was assumed a leading edge half angle of 10°, a circular cylinder diameter of 10^{-2}m and truncated wedge thicknesses t/λ_∞ of 0.01, 0.1 and 1.0, where λ_∞ is the

freestream mean free path. Figure (1a) illustrates schematically this construction. The common body height H and the body length L are obtained in a straightforward manner.

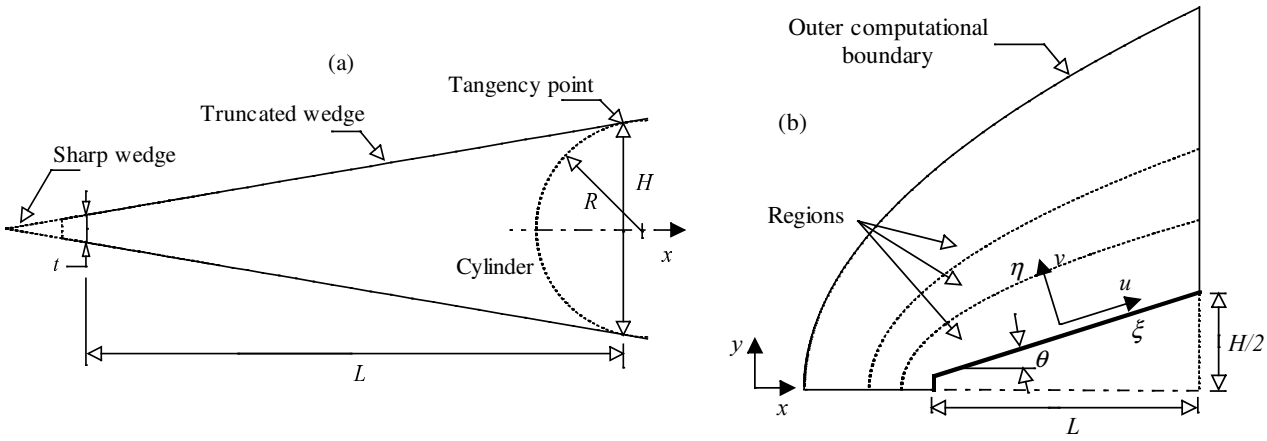

Figure 1: Drawing illustrating (a) the leading edge geometry and (b) the computational domain.

3. Computational Method and Procedure

The Direct Simulation Monte Carlo (DSMC) method, pioneered by Bird (1994), has become one of the standard and reliable successful numerical techniques for modeling complex flows in the transition regime. The transition regime is the category of flow that falls between the continuum regime, where the Navier-Stokes equations are valid, and the free molecular regime, which is the limit of infinite Knudsen number.

In the DSMC method, a group of representative molecules are tracked as they move, collide and undergo boundary interactions in simulated physical space. Each simulated molecule represents a very much larger number of real molecules. The molecular motion, which is considered to be deterministic, and the intermolecular collisions, which are considered to be stochastic, are uncoupled over the small time step used to advance the simulation and computed sequentially.

In this paper, molecular collisions are modeled by the variable hard sphere (VHS) molecular model (Bird, 1981). This model employs the simple hard sphere angular scattering law so that all directions are equally possible for post-collision velocity in the center-of-mass frame of reference. Nevertheless, the collision cross section depends on the relative speed of colliding molecules. The mechanics of the energy exchange processes between kinetic and internal modes for rotation and vibration are controlled by the Borgnakke-Larsen statistical model (Borgnakke and Larsen, 1975). The essential feature of this model is that a part of collisions is treated as completely inelastic, and the remainder of the molecular collisions is regarded as elastic. Simulations are performed using a nonreacting gas model consisting of two chemical species, N_2 and O_2. The vibrational temperature is controlled by the distribution of energy between the translational and rotational modes after an inelastic collision. The probability of an inelastic collision determines the rate at which energy is transferred between the translational and internal modes after an inelastic collision. For a given collision, the probabilities are designated by the inverse of the relaxation numbers, which correspond to the number of collisions necessary, on average, for a molecule to relax. The rates of rotational and vibrational relaxation are dictated by collision numbers Z_R and Z_V, respectively. The collision numbers are traditionally given as constants, 5 for rotation and 50 for vibration.

The physical space is divided into a number of regions, which are subdivided into computational cells. The cells are further subdivided into 4 subcells, 2 subcells/cell in each direction. The cell provides a convenient reference sampling of the macroscopic gas properties, while the collision partners are selected from the same subcell for the establishment of the collision rate. As a result, the flow resolution is much higher than the cell resolution. The dimensions of the cells must be such that the change in flow properties across each cell is small. In particular, cell size in regions of significant flow properties gradients, such as density of temperature gradients, is traditionally chosen to be of the order of the local mean free path or even smaller (Alexander et. al., 1998). The cell size is also made small enough to restrict collisions to nearby particles but should contain a sufficient number of particles so that the method remains statistically accurate. The number of simulated molecules in a cell should be on the order of 20 to avoid distortion of the collision rates.

The computational domain used for the calculation is made large enough so that the upstream and side boundaries can be specified as freestream conditions. The flow at the downstream outflow boundary is predominantly supersonic and vacuum conditions are specified (Bird, 1994). At this boundary, simulated molecules can only exit. Diffuse reflection with complete thermal accommodation is the condition applied to the body surface. A schematic view of the computational domain is depicted in Fig. 1(b). Advantage of the flow symmetry is taken into account, and molecular simulation is applied to one-half of a full configuration in order to reduce the computational domain.

Numerical accuracy in DSMC method depends on the grid resolution chosen as well as the number of particles per

computational cell. Both effects were investigated in order to determine the number of cells and the number of particles required to achieve grid independence solutions for the thermal nonequilibrium flow that arises near the nose of the leading edges. A discussion of both effects on the aerodynamic surface quantities will not be presented due to the relatively small number of pages of this work.

The freestream and flow conditions used in the present calculations are those given by Santos (2002) and summarized in Tab. (1). The gas properties considered in the simulation are shown in Tab. (2). The freestream velocity V_∞, assumed to be constant at 1.49, 2.37 and 3.56 km/s, corresponds to freestream Mach number M_∞ of 5, 8, and 12, respectively. The temperature T_w on the wedge surface is maintained constant at 880 K for all cases considered.

Table 1: Freestream Conditions

Temperature T_∞ (K)	Pressure p_∞ (N/m^2)	Density ρ_∞ (kg/m^3)	Number density n_∞ (m^{-3})	Viscosity μ_∞ (Ns/m^2)	Mean free path λ_∞ (m)
220.0	5.582	8.753 x 10^{-5}	1.8209 x 10^{21}	1.455 x 10^{-5}	9.03 x 10^{-4}

Table 2: Gas Properties

	Mole fraction X	Molecular mass m (kg)	Molecular diameter d (m)	Degree of freedom ζ
O_2	0.237	5.312 x 10^{-26}	4.01 x 10^{-10}	5
N_2	0.763	4.65 x 10^{-26}	4.11 x 10^{-10}	5

The overall Knudsen number Kn is defined as the ratio of the molecular mean free path λ_∞ in the freestream gas to a characteristic dimension of the flowfield. In the present study, the characteristic dimension was defined as being the thickness t of the truncated leading edges. For the thicknesses investigated, t/λ_∞ = 0.01, 0.1 and 1.0, the overall Knudsen numbers correspond to Kn_t = 100, 10 and 1, respectively. The Reynolds number Re_t covers the range from 0.193 to 19.3, based on conditions in the undisturbed stream with leading edge thickness t as the characteristic length.

4. Computational Results and Discussion

Attention is now focused on the calculations of the heat transfer coefficient, total drag and the shock standoff distance obtained from the DSMC results. The purpose of this section is to discuss and to compare differences in the profiles of these properties due to variations on the freestream Mach number and on the leading edge thickness.

4.1. Heat Transfer Coefficient

The heat transfer coefficient C_h is defined as being,

$$C_h = \frac{q_w}{\frac{1}{2}\rho_\infty V_\infty^3} \tag{1}$$

where the heat flux q_w to the wedge surface is calculated by the net energy fluxes of the molecules impinging on the surface. A flux is regarded as positive if it is directed toward the surface. The net heat flux q_w is related to the sum of the translational, rotational and vibrational energies of both incident and reflected molecules as defined by,

$$q_w = q_i + q_r = \sum_{j=1}^{N} \left\{ \left[\frac{1}{2} m_j c_j'^2 + e_{Rj} + e_{Vj} \right]_i + \left[\frac{1}{2} m_j c_j'^2 + e_{Rj} + e_{Vj} \right]_r \right\} \tag{2}$$

where N is the number of molecules colliding with the surface by unit time and unit area, m is the mass of the molecules, c' is the thermal velocity of the molecules, e_R and e_V stand for the rotational and vibrational energies, respectively. Subscripts i and r refer to incident and reflected molecules.

The compressibility effect on the heat transfer coefficient is plotted in Figs. (2), (3) and (4) for leading edge thicknesses t/λ_∞ of 0.01, 0.1, 1.0, respectively. Plots on the left side correspond to the heat transfer coefficient on the front surface as a function of the dimensionless height y/λ_∞, measured from the stagnation point up to the shoulder of the wedge, and plots on the right side correspond to the heat transfer coefficient to the inclined surface of the wedge as a function of the dimensionless arc length s/λ_∞, measured from the shoulder of the leading edge. For purpose of comparison, this set of Figs. presents the free molecular flow (FM) limit value for the heat transfer coefficient by assuming free collision flow (Bird, 1994).

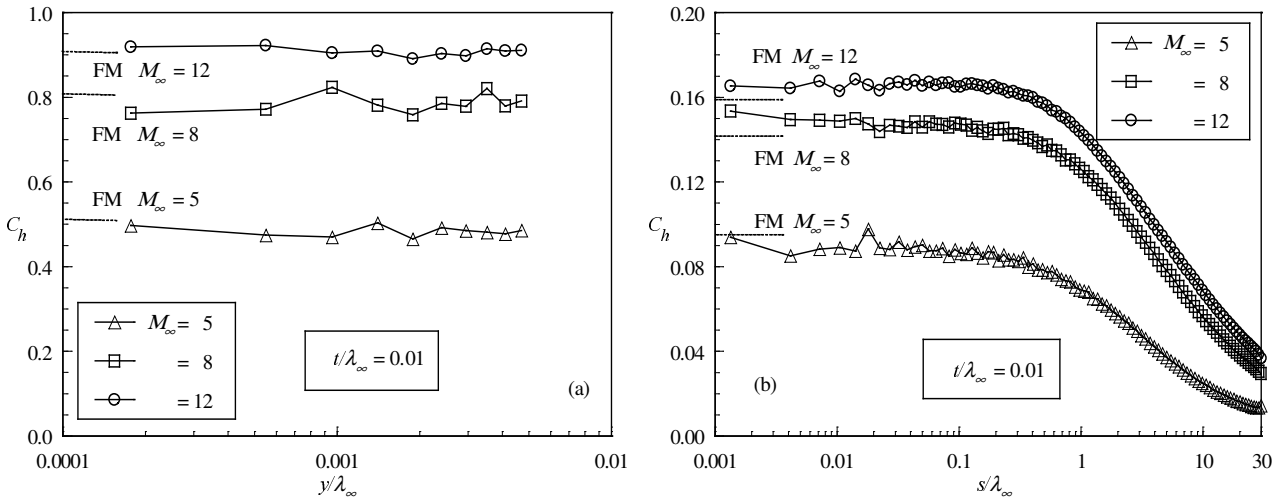

Figure 2: Heat transfer coefficient C_h along the (a) front surface and (b) along the inclined surface of the wedge as a function of the Mach number for the $t/\lambda_\infty = 0.01$ case.

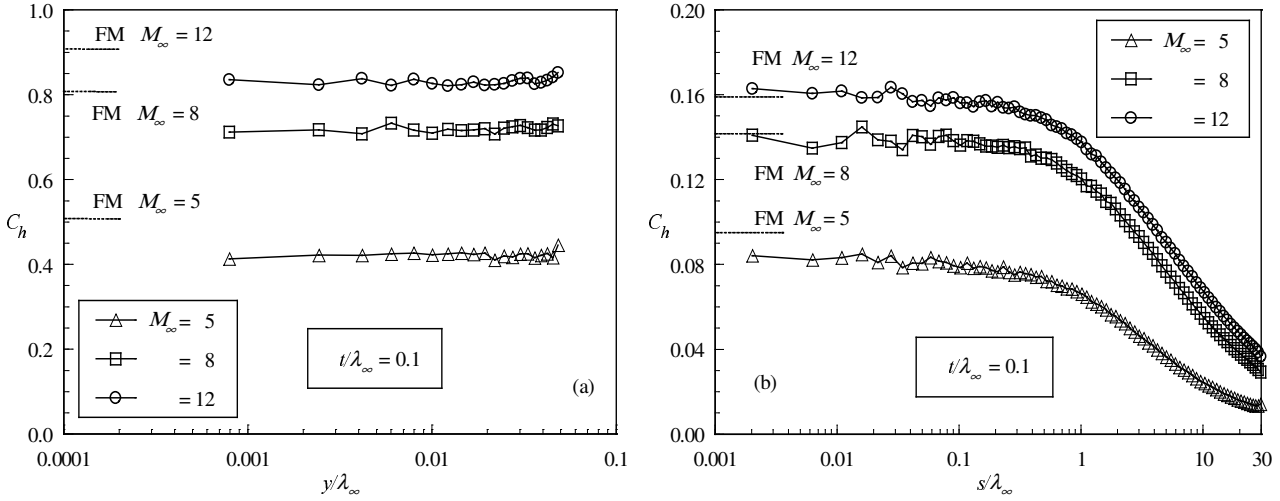

Figure 3: Heat transfer coefficient C_h along the (a) front surface and (b) along the inclined surface of the wedge as a function of the Mach number for the $t/\lambda_\infty = 0.1$ case.

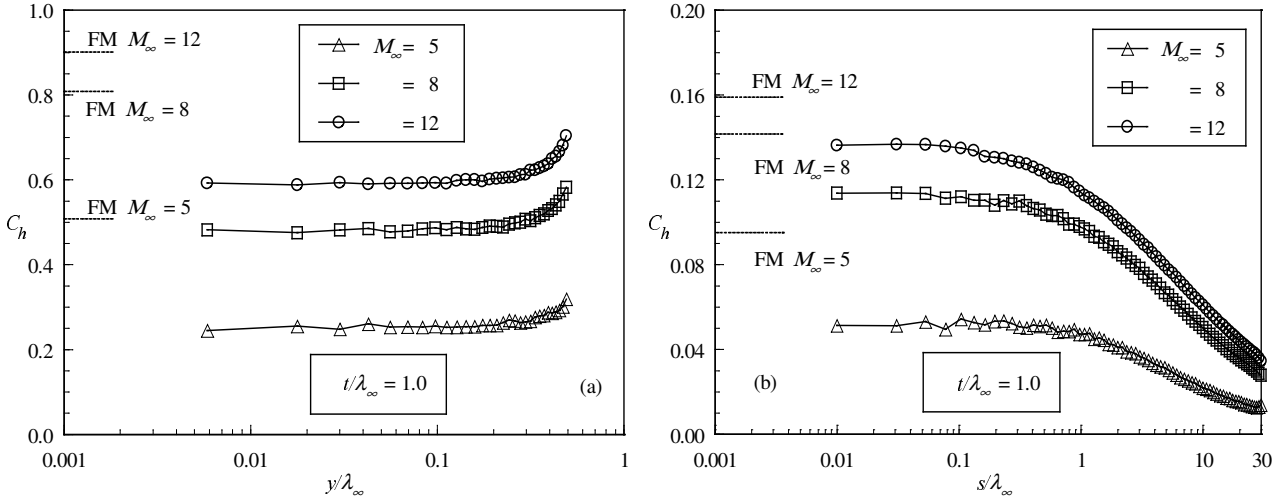

Figure 4: Heat transfer coefficient C_h along the (a) front surface and (b) along the inclined surface of the wedge as a function of the Mach number for the $t/\lambda_\infty = 1.0$ case.

According to Figs. (2), (3) and (4), it is seen that the heat transfer coefficient changes on the front and inclined surfaces of the wedge with increasing freestream Mach number. As the freestream Mach number increases from 5 to 12, the kinetic energy of the freestream molecules increases. As a result, the heat flux to the body surface increases. This behavior is better visualized in Eq. (2). The incident component of the thermal velocity c' of the molecules is a function of the freestream Mach number. However, the reflected component of the thermal velocity is not a function of the freestream Mach number. Due to the diffuse reflection model, the reflected component of the velocity is obtained from a Maxwellian distribution that only takes into account for the temperature of the body surface, which has the same value for the freestream Mach number range investigated. It also should be emphasized that the number of molecules colliding with the surface by unit time and unit area, which appears in Eq. (2), is the same for the incident and reflected components of the heat transfer coefficient. Nevertheless, it dramatically increases in the front surface of the leading edges with increasing the freestream Mach number (not shown).

Referring to Figs. (2), (3) and (4), it is also observed that the heat transfer coefficient is sensitive to the leading edge thickness. As would be expected, the blunter the leading edge is the lower the heat transfer coefficient along the front surface. For the bluntest case investigated, t/λ_∞ = 1.0, the heat transfer coefficient increases in the vicinity of the shoulder. This behavior would be also expected since the thermal velocity of the molecules increases in the vicinity of the shoulder on the front surface, where the flow is allowed to expand. In addition, the contribution of the translational energy to the net heat flux varies with the square of the thermal velocity of the molecules, as shown in Eq. (2).

4.2. Total Drag Coefficient

The drag on a surface in a gas flow results from the interchange of momentum between the surface and the molecules colliding with the surface. The total drag is obtained by the integration of the pressure p_w and shear stress τ_w distributions along the wedge surface. In an effort to understand the nature of the pressure and shear stress forces acting on the surface of the truncated leading edges, both forces will be presented in this section.

The pressure p_w on the wedge surface is calculated by the sum of the normal momentum fluxes of both incident and reflected molecules at each time step as follows,

$$p_w = p_i + p_r = \sum_{j=1}^{N} \left\{ \left[m_j c_{\eta j}'^2 \right]_i + \left[m_j c_{\eta j}'^2 \right]_r \right\} \tag{3}$$

where c_η' is the normal component of the thermal velocity of the molecules.

The sensitivity of the wall pressure to variations on the freestream Mach number is demonstrated in Fig. (5), normalized by the freestream pressure p_∞, for leading edge thickness t/λ_∞ of 0.01. Figure (5a) shows the dimensionless wall pressure on the front surface as a function of the dimensionless height y/λ_∞. The dimensionless wall pressure along the inclined surface of the wedge is plotted in Fig. (5b) as a function of the dimensionless arc length s/λ_∞, measured from the shoulder of the leading edge. Plotted along with the computational solutions for dimensionless wall pressure is the wall pressure limit predicted by the free molecular flow, which corresponds to the case at infinite Knudsen number.

Referring to Fig. (5a), it can be seen that the front surface experiences a remarkable pressure. The pressure is basically constant along the front surface, and increases the constant value with increasing the freestream Mach number. Also, the wall pressure reaches the limit values predicted by free molecular flow as expected, since for the t/λ_∞ = 0.01 case the overall Knudsen number is Kn_t = 100. In contrast, according to Fig. (5b), the wall pressure on the inclined surface of the wedge is far from the limit value predicted by the free molecular flow. It is also seen that the wall pressure on the inclined surface is one order of magnitude smaller than that on the front surface.

The general shape of the wall pressure is basically similar to the other two cases investigated, as displayed in Figs. (6) and (7) for leading edge thicknesses t/λ_∞ of 0.1 and 1.0, respectively. By comparing Figs. (5a), (6a) and (7a), it is observed that the maximum pressure reached on the front surface is obviously decreased by an increase in the leading edge thickness. As the leading edge thickness increases, the nose of the leading edge becomes blunter and a rather different flow behavior is seen, as shown in Fig. (7b) where the wall pressure for the t/λ_∞ = 1.0 case does not display the same structure as those presented by the t/λ_∞ = 0.01 and 0.1 cases.

The shear stress τ_w on the body surface is calculated by averaging the tangential momentum transfer of the molecules impinging on the surface. For the diffuse reflection model imposed for the gas-surface interaction, reflected molecules have a tangential moment equal to zero, since the molecules essentially lose, on average, their tangential velocity component. In this fashion, the tangential momentum flux of the incident molecules is defined as follows,

$$\tau_w = \sum_{j=1}^{N} m_j c_{\xi j}'^2 \tag{4}$$

where c_ξ' is the tangential component of the thermal velocity of the molecules.

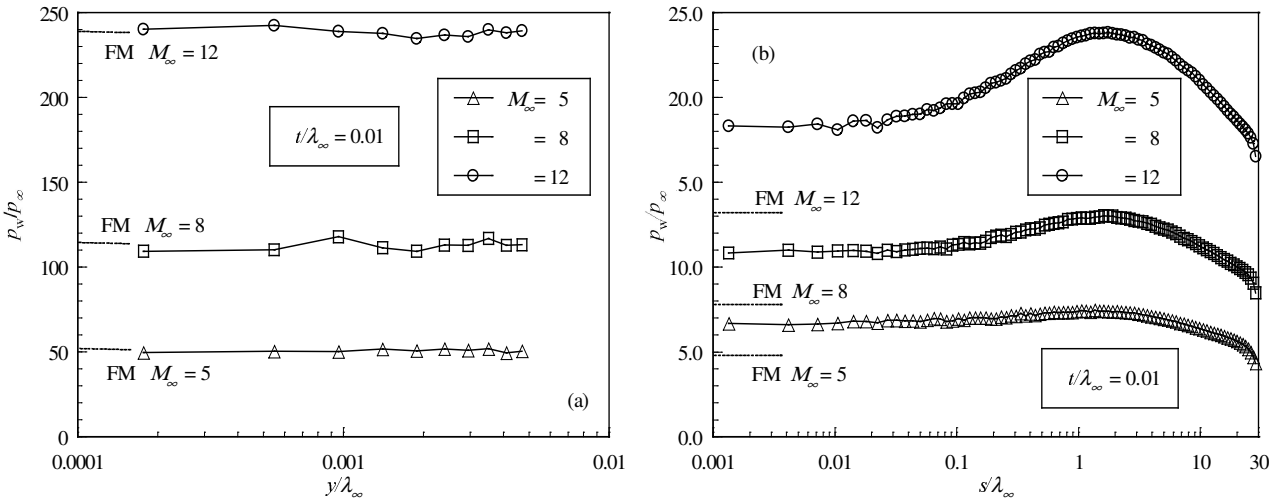

Figure 5: Dimensionless wall pressure p_w/p_∞ acting on the (a) front surface and (b) on the inclined surface of the wedge as a function of the Mach number for the $t/\lambda_\infty = 0.01$ case.

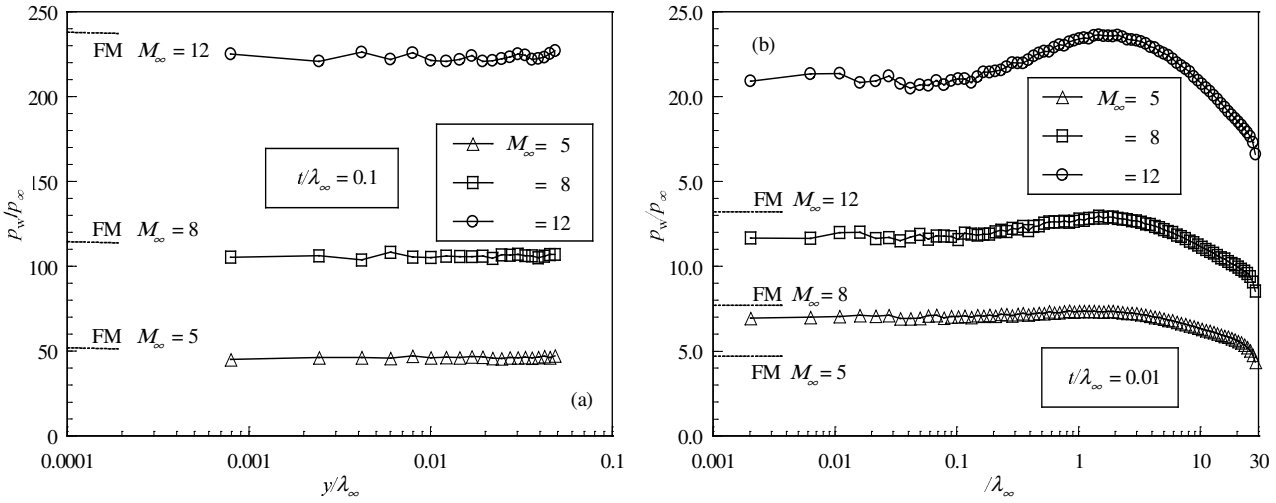

Figure 6: Dimensionless wall pressure p_w/p_∞ acting on the (a) front surface and (b) on the inclined surface of the wedge as a function of the Mach number for the $t/\lambda_\infty = 0.1$ case.

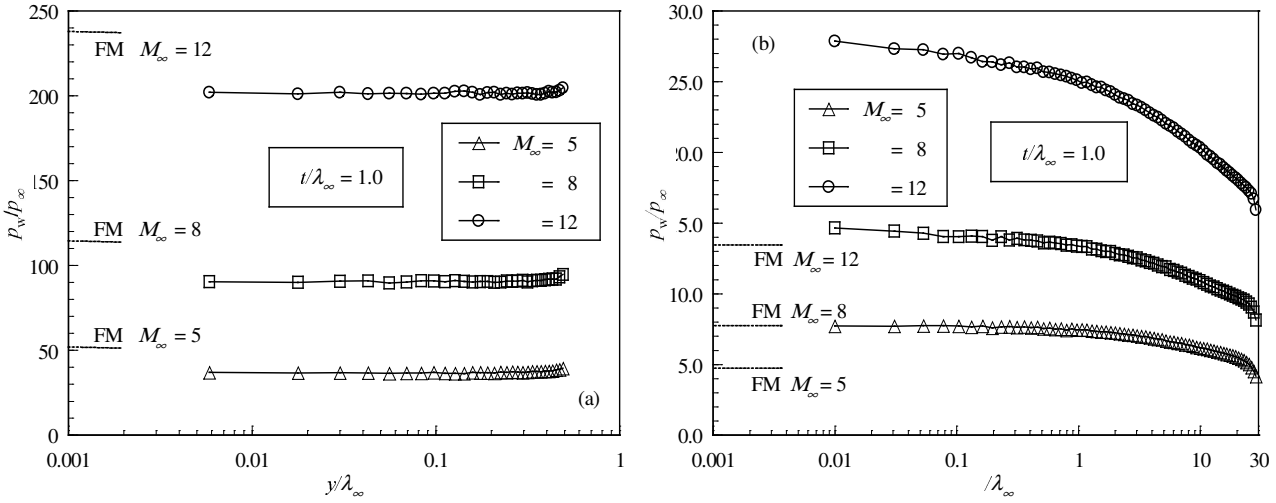

Figure 7: Dimensionless wall pressure p_w/p_∞ acting on the (a) front surface and (b) on the inclined surface of the wedge as a function of the Mach number for the $t/\lambda_\infty = 1.0$ case.

Distributions of the shear stress, normalized by the freestream pressure p_∞, along the wedge surface at different freestream Mach number are displayed in Figs. (8), (9) and (10) for leading edge thicknesses t/λ_∞ of 0.01, 0.1 and 1.0, respectively. Figures (8a), (9a) and (10a) illustrate the dimensionless shear stress on the front surface and Figs. (8b), (9b) and (10b) depict the dimensionless shear stress on the inclined surface of the wedge.

On the front surface, the distributions of the dimensionless shear stress for all thicknesses are nearly identical. It is zero at the stagnation point and increases along the front surface up to the shoulder of the wedge. The value of τ_w/p_∞ appreciably increases near the shoulder of the wedge with increasing the thickness of the leading edge. The trend of the distributions on the front surface is as expected since the velocity of the molecules increases in the vicinity of the shoulder due to the flow expansion. As a result, the tangent momentum of the molecules increases in this region, even though the number of molecules impinging on the front surface decreases in the vicinity of the shoulder (not shown).

On the afterbody surface, the general shape of the shear stress on the wedge surface is similar to that for the heat flux. Another interesting feature in the shear stress is that it is the same order of magnitude on both surfaces, in contrast to the pressure and heat transfer coefficients.

The total drag coefficient C_d is defined as being,

$$C_d = \frac{D}{\frac{1}{2}\rho_\infty V_\infty^2 H} = \frac{D/p_\infty}{\frac{1}{2}\gamma M_\infty^2 H} \tag{5}$$

where D is the resultant force acting on the body surface, γ is the specific heat ratio and H is the height at the matching point common to the leading edges (see Fig. (1a)).

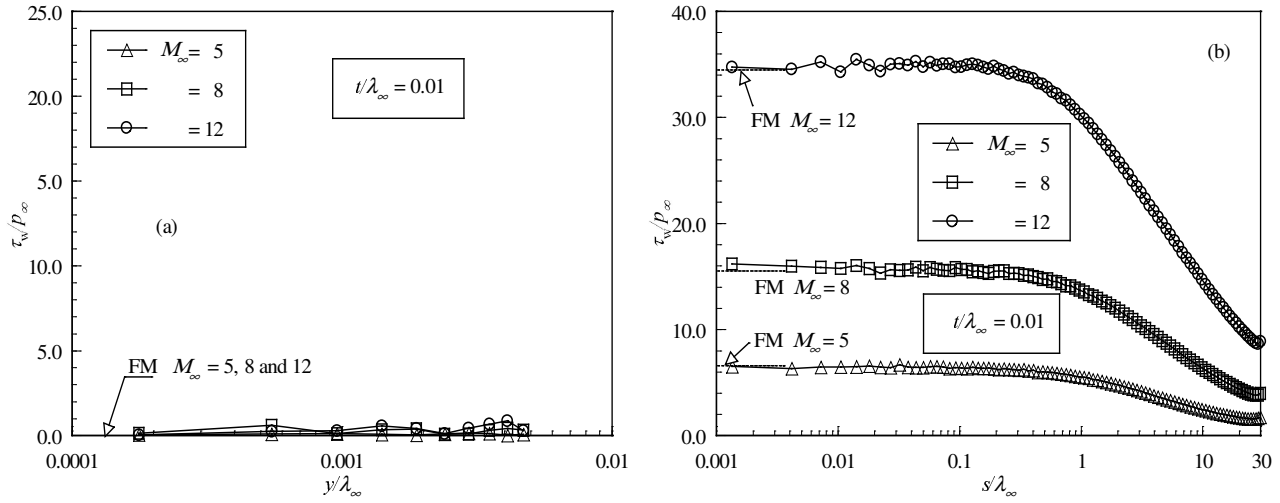

Figure 8: Dimensionless shear stress τ_w/p_∞ acting on the (a) front surface and (b) on the inclined surface of the wedge as a function of the Mach number for the $t/\lambda_\infty = 0.01$ case.

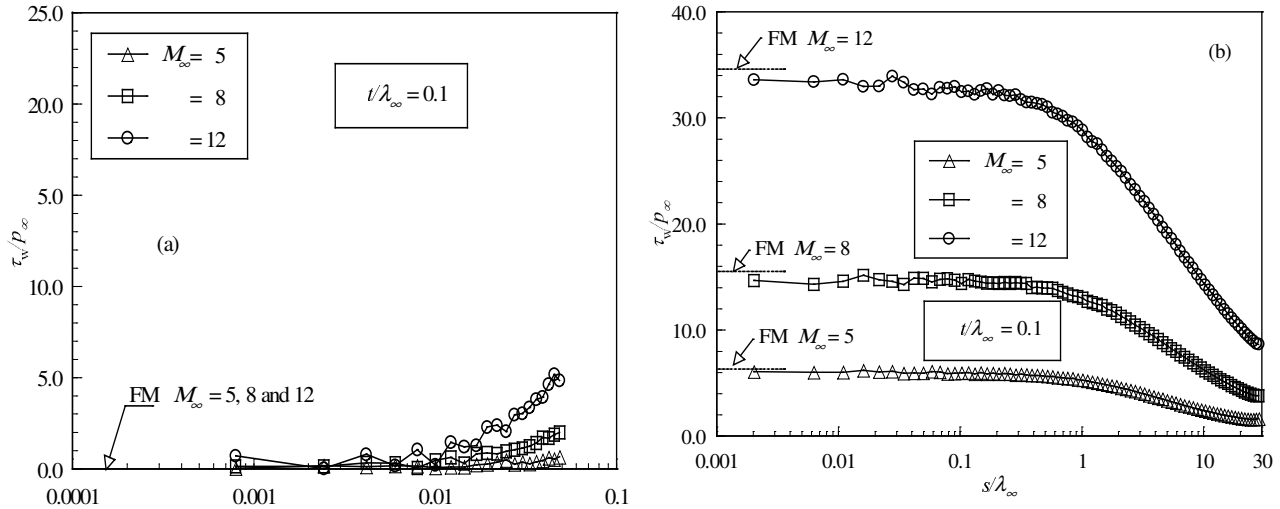

Figure 9: Dimensionless shear stress τ_w/p_∞ acting on the (a) front surface and (b) on the inclined surface of the wedge as a function of the Mach number for the $t/\lambda_\infty = 0.1$ case.

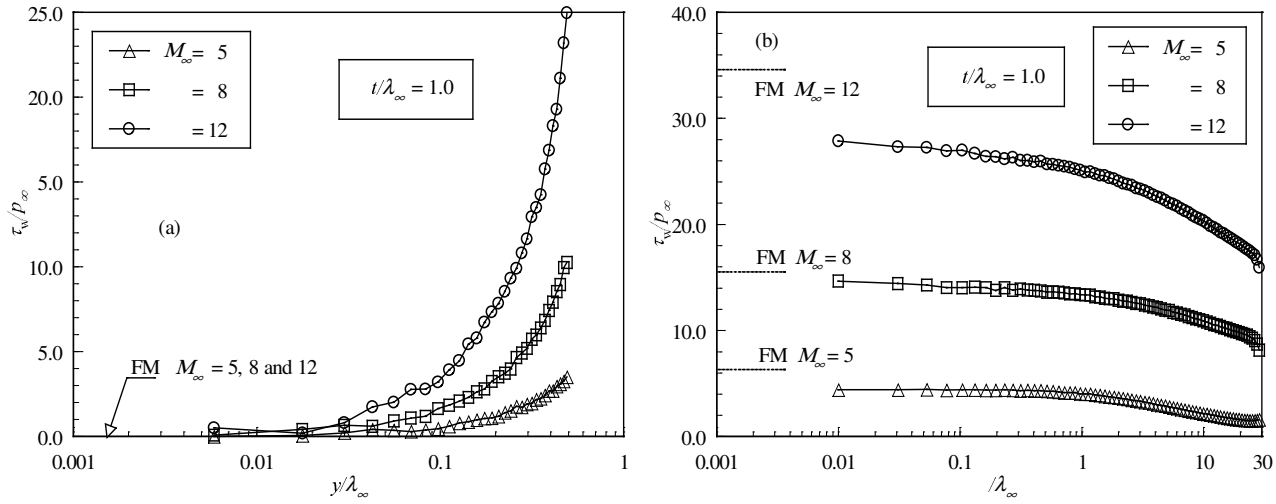

Figure 10: Dimensionless shear stress τ_w/p_∞ acting on the (a) front surface and (b) on the inclined surface of the wedge as a function of the Mach number for the $t/\lambda_\infty = 1.0$ case.

The resultant force acting on the wedge was obtained by the integration of the pressure p_w and shear stress τ_w distributions from the stagnation point of the leading edge to the station L that corresponds to the tangent point common to all wedges (see Fig. (1)). It is worthwhile to mention that the values for the total drag coefficient were obtained by assuming the shapes acting as leading edges. As a result, no base pressure effects were taken into account on the calculations. The DSMC results for total drag coefficient are presented as total drag coefficient C_d and its components of pressure drag coefficient C_{pd} and skin friction drag coefficient C_{fd} on Tab. (3).

According to Tab. (3), it can be seen that as the leading edge becomes blunt the contribution of the pressure drag coefficient to the total drag coefficient increases and the contribution of the skin friction drag coefficient decreases. As the net effect on total drag coefficient depends on these two opposite behaviors, hence no appreciable changes are observed in the total drag coefficient for the leading edge thicknesses investigated, by considering the same freestream Mach number. As a reference, for freestream Mach number of 5, the pressure drag is 30% and 44.3% of the total drag for the leading edge thicknesses t/λ_∞ of 0.01 and 1.0, respectively. On the other hand, the skin friction contribution decreases from 70% to 55.7% for the same cases. This behavior appears to be fully explained through the changes in pressure and shear stress shown in Figs. (5)-(10). Note that on the front surface, for the same freestream Mach number, the wall pressure slightly decreases as the leading edge thickness increases, while it tends to increase on the inclined surface of the wedge. In contrast, the shear stress has no contribution on the front surface and it decreases on the afterbody surface.

Significant differences in total drag coefficient between freestream Mach number of 5 and 12 are seen on the leading edge shapes. By referring to Tab. (3), the total drag coefficient decreases around 15% as the freestream Mach number increases from 5 to 12, despite of the fact that the wall pressure and shear stress increase with freestream Mach number significantly, as depicted in Figs. (5) to (10). Equation (5) provides the necessary assistance in order to understand this behavior. The numerator of Eq. (5) grows with wall pressure and shear stress, while the denominator ($\propto M_\infty^2$) increases faster than the numerator and results in a total drag coefficient decrease.

In order to better visualize the behavior of the total drag coefficient shown on Tab. (3), Fig. (11) displays the pressure drag, skin friction drag and the total drag coefficients as a function of the freestream Mach number. Figure (11a) refers to the leading edge thickness t/λ_∞ of 0.01 and Fig. (11b) to leading edge thickness t/λ_∞ of 1.0.

Table 3: Pressure drag, skin friction drag and total drag coefficients.

	$t/\lambda_\infty = 0.01$			$t/\lambda_\infty = 0.1$			$t/\lambda_\infty = 1.0$		
	$M_\infty = 5$	$M_\infty = 8$	$M_\infty = 12$	$M_\infty = 5$	$M_\infty = 8$	$M_\infty = 12$	$M_\infty = 5$	$M_\infty = 8$	$M_\infty = 12$
C_{pd}	0.339	0.238	0.197	0.358	0.255	0.214	0.504	0.402	0.362
C_{fd}	0.790	0.774	0.784	0.770	0.757	0.767	0.634	0.624	0.635
C_d	1.129	1.012	0.981	1.128	1.011	0.981	1.138	1.025	0.997
% C_{pd}/C_d	30.0	23.5	20.0	31.7	25.2	21.8	44.3	39.2	36.3
% C_{fd}/C_d	70.0	76.5	80.0	68.3	74.8	78.2	55.7	60.8	63.7

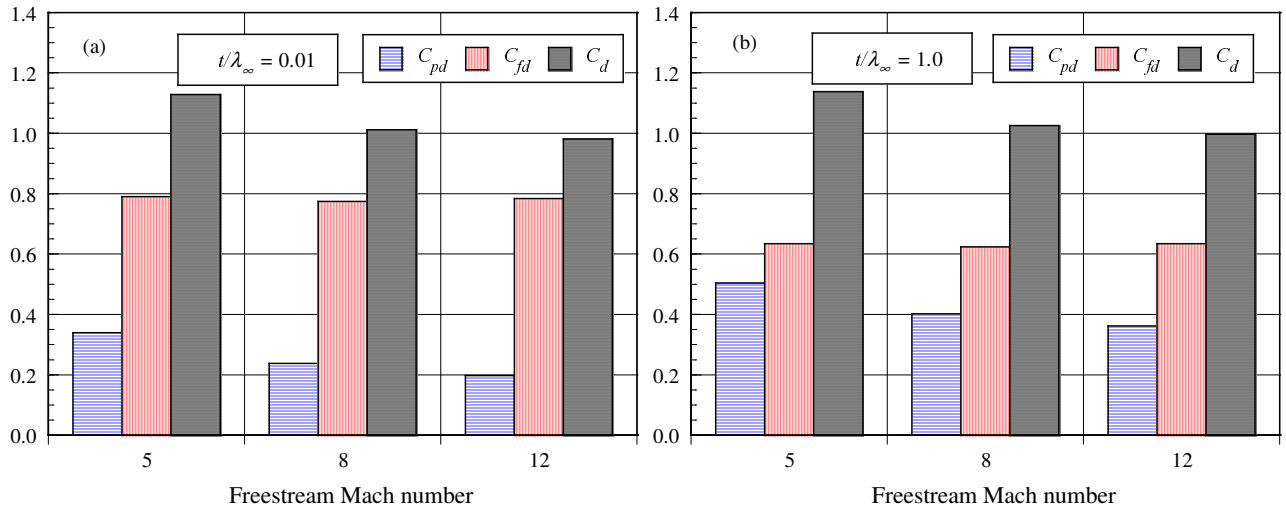

Figure 11: Pressure drag, skin friction drag and total drag coefficients as a function of the freestream Mach number for leading edge thickness t/λ_∞ of (a) 0.01 and (b) 1.0.

4.3. Shock Wave Standoff Distance

The problem of predicting the shape and location of detached shock waves has been stimulated by the necessity for blunt noses and leading edges configurations designed for hypersonic flight in order to cope with the aerodynamic heating. Also, the ability to predict the shape and location of shock waves is of primary importance in analysis of aerodynamic interference. In this context, the intent in this section is to present the shock wave standoff distance (location) obtained from the numerical simulations.

In a rarefied flow, the shock wave has a finite region that depends on the transport properties of the gas, and can no longer be considered as a discontinuity obeying the classical Rankine-Hugoniot relations. In this scenario, the shock standoff distance is defined as being the distance between the shock wave center and the nose of the leading edge along the stagnation streamline.

In order to quantify the shock standoff distance, the shock wave center is determined by employing the following procedure (Santos, 2003): the flow is assumed to consist of three distinct classes of molecules; those molecules from the freestream that have not been affected by the presence of the leading edge are denoted as class I molecules; those molecules that, at some time in their past history, have struck and been reflected from the body surface are denoted as class II molecules; and those molecules that have been indirectly affected by the presence of the body are defined as class III molecules.

It is assumed that the class I molecule changes to class III molecule when it collides with class II or class III molecule. Class I or class III molecule is progressively transformed into class II molecule when it interacts with the body surface. Also, a class II molecule remains class II regardless of subsequent collisions and interactions. Hence, the transition from class I molecules to class III molecules may represent the shock wave, and the transition from class III to class II defines the boundary layer.

For illustration purpose, the distribution of molecules for each class along the stagnation streamline is demonstrated in Fig. (12a) for the t/λ_∞ = 1.0 case and freestream Mach number of 12. η/λ_∞ is the dimensionless distance away from the body (see Fig. (1b)), and f is the ratio of the number of molecules for each one of the classes to the total amount of molecules inside each cell. The shock wave center is obtained by calculating the position that corresponds to the maximum value f for class III molecules in the η-direction. The shock wave standoff distance δ, defined as being the distance from the shock wave center to the nose of the leading edge along the stagnation streamline, can be observed in Fig. (12a). Table (4) displays the shock standoff distance, normalized by λ_∞, for all cases investigated, and Fig. (12b) depicts the dimensionless standoff distance δ/λ_∞ as a function of the freestream Mach number.

As is observed in Tab. (4) and Fig. (12b), there is a discrete shock standoff distance for all cases investigated. The results tend to confirm the expectation that the shock standoff distance increases not only with decreasing the freestream Mach number but also with increasing the leading edge thickness, i.e., as the leading edge bluntness increases.

Table 4: Dimensionless shock wave standoff distance δ/λ_∞.

	$t/\lambda_\infty = 0.01$	$t/\lambda_\infty = 0.1$	$t/\lambda_\infty = 1.0$
$M_\infty = 5$	0.130	0.241	0.818
$M_\infty = 8$	0.073	0.221	0.666
$M_\infty = 12$	0.070	0.220	0.597

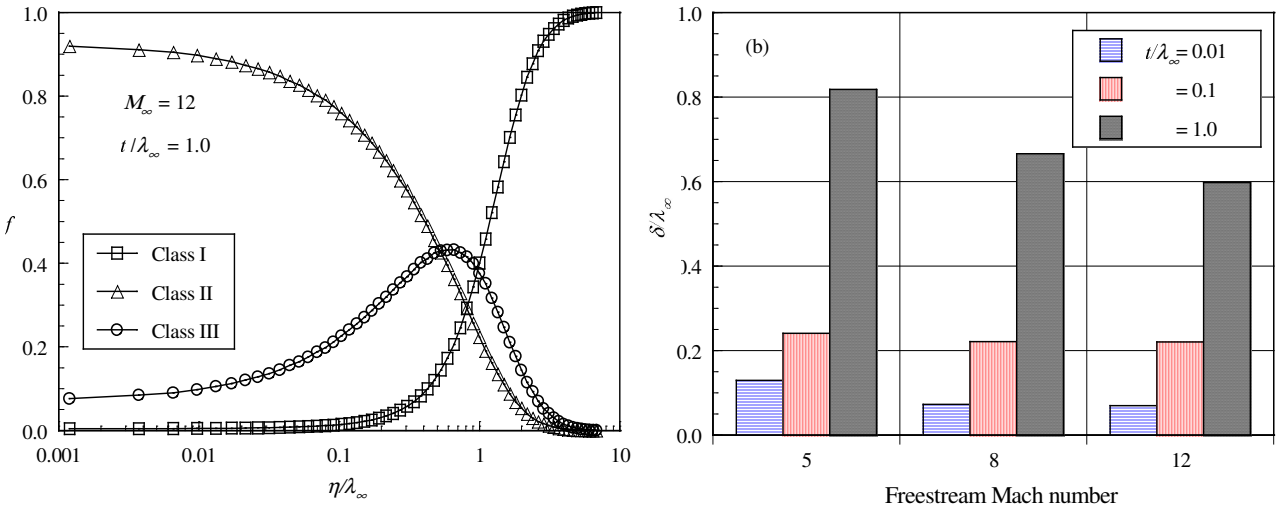

Figure 12: (a) Distribution of molecules for classes I, II and III along the stagnation stream line for the t/λ_∞ = 1.0 case and Mach number of 12, and (b) dimensionless shock standoff distance δ/λ_∞ as a function of the Mach number.

5. Concluding Remarks

This study applies the Direct Simulation Monte Carlo method to investigate rarefied gas over truncated wedges. Effects of air speed on the heat transfer coefficient, drag coefficient and shock standoff distance for wide ranges of parameters are examined. The freestream Mach number is varied from 5 to 12, and the Knudsen number, based on the thickness of the leading edges, ranges between 1 and 100. Cases considered in this study cover the hypersonic flow in the transitional and free molecular regimes.

Performance results for leading edge thickness t/λ_∞ of 0.01 indicated that the flow approaches the free molecular flow in the vicinity of the front surface, for the freestream Mach number considered. Substantial changes in the aerodynamic surface quantities were observed as the leading edge thickness increased. It was found that the total drag coefficient presented almost the same values for a fixed freestream Mach number. However, as expected it decreased as the freestream Mach number increased.

Results indicated that, with the size of the models being tested in hypersonic tunnels, large effects on flow structure and surface quantities due to leading edge thickness are possible even with models whose leading edges are generally considered as being aerodynamically sharp.

6. References

Alexander, F. J., Garcia, A. J. and Alder, B. J., 1998, "Cell Size Dependence of Transport Coefficients in Stochastic Particle Algorithms", Physics of Fluids, Vol. 10, pp. 1540-1542.

Anderson, J. L., 1990, "Tethered Aerothermodynamic Research for Hypersonic Waveriders", Proceedings of the 1st International Hypersonic Waverider Symposium, Univ. of Maryland, College Park, MD.

Bird, G. A., 1981, "Monte Carlo Simulation in an Engineering Context", Progress in Astronautics and Aeronautics: Rarefied gas Dynamics, Ed. Sam S. Fisher, Vol. 74, part I, AIAA New York, pp. 239-255.

Bird, G. A., 1994, "Molecular Gas Dynamics and the Direct Simulation of Gas Flows", Oxford University Press, Oxford, England, UK.

Borgnakke, C. and Larsen, P. S., 1975, "Statistical Collision Model for Monte Carlo Simulation of Polyatomic Gas Mixture", Journal of computational Physics, Vol. 18, pp. 405-420.

Graves, R. E. and Argrow, B. M., 2001, "Aerodynamic Performance of an Osculating-Cones Waverider at High Altitudes", 35th AIAA Thermophysics Conference, Paper AIAA 2001-2960, Anaheim, CA.

Haas, B. L., Fallavollita, M. A., 1994, "Flow Resolution and Domain Influence in Rarefied Hypersonic Blunt-Body Flows", Journal of Thermophysics and Heat Transfer, Vol. 8(4), pp. 751-757.

Potter, J. L. and Rockaway, J. K., 1994, "Aerodynamic Optimization for HypersonicFlight at Very High Altitudes", Rarefied Gas Dynamics: Space Sciences and Engineering, Progess in Astronautics and Aeronautics, vol. 160,, Ed. B. D. Shizgal and D. P. Weaver, pp. 296-307.

Rault, D. F. G., 1994, "Aerodynamic Characteristics of a Hypersonic Viscous Optimized Waverider at High Altitude", Journal of Spacecraft and Rockets, Vol. 31(5), pp. 719-727.

Santos, W. F. N., 2002, "Truncated Leading Edge Effects on Flowfield Structure of a Wedge in Low Density Hypersonic Flight Speed", Proceedings of the 9th Brazilian Congress of Thermal Engineering and Sciences, Paper CIT02-0879, Caxambu, MG, Brazil.

Santos, W. F. N., 2003, "Shock Wave Shape on Power Law Leading Edges", Proceedings of the 24th International Symposium on Shock Waves, July 20-25, 2003, Beijing, China (to appear).